Biomedical Optics EXPRESS

Photoacoustic tomography system for noninvasive real-time three-dimensional imaging of epilepsy

Bo Wang,[1] Liangzhong Xiang,[1] Max S. Jiang,[1] Jianjun Yang,[1] Qizhi Zhang,[1] Paul R. Carney,[1,2,3,4,5] and Huabei Jiang[1,*]

[1]*J. Crayton Pruitt Family Department of Biomedical Engineering, University of Florida, Gainesville, FL 32611, USA*
[2]*Department of Pediatrics, University of Florida, Gainesville, FL 32611, USA*
[3]*Neurology and Neuroscience, University of Florida, Gainesville, FL 32611, USA*
[4]*Wilder Center of Excellence for Epilepsy Research, University of Florida, Gainesville, FL 32611, USA*
[5]*McKnight Brain Institute, University of Florida, Gainesville, FL 32611, USA*
**hjiang@bme.ufl.edu*

Abstract: A real-time three-dimensional (3D) photoacoustic imaging system was developed for epilepsy imaging in small animals. The system is based on a spherical array containing 192 transducers with a 5 MHz central frequency. The signals from the 192 transducers are amplified by 16 homemade preamplifier boards with 26 dB and multiplexed into a 64 channel data acquisition system. It can record a complete set of 3D data at a frame rate of 3.3 f/s, and the spatial resolution is about 0.2 mm. Phantom experiments were conducted to demonstrate the high imaging quality and real time imaging ability of the system. Finally, we tested the system on an acute epilepsy rat model, and the induced seizure focus was successfully detected using this system.

OCIS codes: (110.5120) Photoacoustic imaging; (170.6920) Time-resolved imaging.

References and links

1. R. A. Kruger, R. B. Lam, D. R. Reinecke, S. P. Del Rio, and R. P. Doyle, "Photoacoustic angiography of the breast," Med. Phys. **37**(11), 6096–6100 (2010).
2. A. A. Karabutov, E. Savateeva, and A. Oraevsky, "Imaging of layered structures in biological tissues with opto-acoustic front surface transducer," Proc. SPIE **3601**, 284–295 (1999).
3. J. Xiao, L. Yao, Y. Sun, E. S. Sobel, J. He, and H. Jiang, "Quantitative two-dimensional photoacoustic tomography of osteoarthritis in the finger joints," Opt. Express **18**(14), 14359–14365 (2010).
4. X. Wang, Y. Pang, G. Ku, G. Stoica, and L. V. Wang, "Three-dimensional laser-induced photoacoustic tomography of mouse brain with the skin and skull intact," Opt. Lett. **28**(19), 1739–1741 (2003).
5. Q. Zhang, Z. Liu, P. R. Carney, Z. Yuan, H. Chen, S. N. Roper, and H. Jiang, "Non-invasive imaging of epileptic seizures in vivo using photoacoustic tomography," Phys. Med. Biol. **53**(7), 1921–1931 (2008).
6. J. Gamelin, A. Maurudis, A. Aguirre, F. Huang, P. Guo, L. V. Wang, and Q. Zhu, "A real-time photoacoustic tomography system for small animals," Opt. Express **17**(13), 10489–10498 (2009).
7. D. W. Yang, D. Xing, S. H. Yang, and L. Z. Xiang, "Fast full-view photoacoustic imaging by combined scanning with a linear transducer array," Opt. Express **15**(23), 15566–15575 (2007).
8. S. Manohar, A. Kharine, J. C. G. van Hespen, W. Steenbergen, and T. G. van Leeuwen, "Photoacoustic mammography laboratory prototype: imaging of breast tissue phantoms," J. Biomed. Opt. **9**(6), 1172–1181 (2004).
9. T. N. Erpelding, Y. Wang, L. Jankovic, Z. Guo, J. Robert, G. David, C. Kim, and L. V. Wang, "Three-dimensional photoacoustic imaging with a clinical two-dimensional matrix ultrasound transducer," Proc. SPIE **7899**, 78990A, 78990A-6 (2011).
10. M. B. Roumeliotis, I. Kosik, and J. J. L. Carson, "3D photoacoustic imaging using staring, sparse array with 60 transducers," Proc. SPIE **8223**, 82233F, 82233F-6 (2012).
11. C. G. A. Hoelen and F. F. M. de Mul, "Image reconstruction for photoacoustic scanning of tissue structures," Appl. Opt. **39**(31), 5872–5883 (2000).
12. L. Yao and H. Jiang, "Photoacoustic image reconstruction from few-detector and limited-angle data," Biomed. Opt. Express **2**(9), 2649–2654 (2011).
13. L. Yao and H. Jiang, "Enhancing finite element-based photoacoustic tomography using total variation minimization," Appl. Opt. **50**(25), 5031–5041 (2011).

#163569 - $15.00 USD Received 27 Feb 2012; revised 19 Apr 2012; accepted 15 May 2012; published 17 May 2012

1. Introduction

Photoacoustic tomography (PAT) is a hybrid method that is capable of imaging optical absorption of tissue through the detection of ultrasound waves generated by a short laser pulse due to transient thermoelastic expansion. It has an imaging resolution that is superior to pure optical imaging at centimeter scale depths. To date PAT has been applied to the detection of breast cancer, skin cancer and osteoarthritis in humans [1–3], and functional brain imaging in small animals [4,5].

For small animal brain imaging, most prior PAT studies were mostly based on a single-transducer scanning system or a circular or linear array of transducers for only 2D imaging [5–7], and the scanning in z direction is needed for 3D imaging purpose, which leads to a non-optimal elevational resolution in the z direction. 2D planar array of transducers has recently been employed for 3D PAT imaging [8,9]. However, due to the limited aperture of 2D planar array transducers, features with high aspect ratio or with orientations oblique to the transducer surface suffer from distortion, and the azimuthal resolution is reduced. Thus, 2D planar array of transducers is not suitable for small animal brain imaging.

Compared to a 2D planar array, a spherical array can offer more complete angular views of the object, providing both high resolution and accurate feature definition regardless of shape or location of the object. The use of sparse spherical arrays for 3D PAT imaging has been recently reported [1,10], but due to the insufficient number of transducers used, these arrays were not designed for small animal brain imaging. The goal of this work is to present a sparse spherical array based PAT system that is specifically designed for real time 3D imaging of small animal brains. The work is a natural extension/improvement of our previous work which reported for the first time 2D PAT imaging of epileptic focus in small animals [5]. The current PAT system is based on a 2D spherical array of 196 transducers coupled with parallel data acquisition, offering a temporal resolution of 0.33 s for data acquisition. We demonstrate this system using static/dynamic phantom and *in vivo* animal experiments. To the best of our knowledge, this is the first work reporting 3D PAT imaging of epileptic focus in small animals.

2. System descriptions

Figure 1 depicts the block diagram of our real-time 3D PAT system. A Ti:sapphire laser optically pumped with a Q-switched Nd:YAG laser sent 8–12 ns pulses at 10 Hz with a wavelength tunable from 690 to 1015 nm. The beam was delivered with an optical fiber

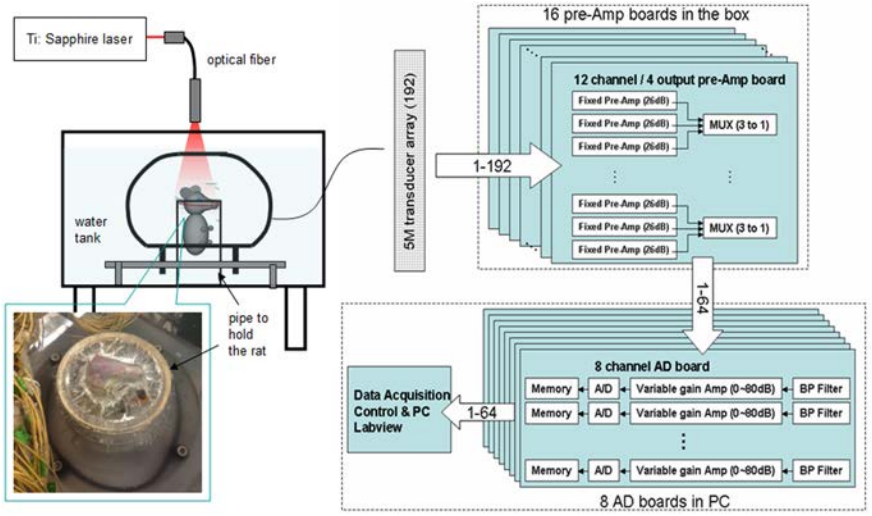

Fig. 1. Block diagram of our real-time 3D PAT system. The inset is a photograph of the close-up view of the chamber holding the rat head.

#163569 - $15.00 USD Received 27 Feb 2012; revised 19 Apr 2012; accepted 15 May 2012; published 17 May 2012

through an opening on the top of the transducer array and produced an approximately uniform illumination in a 2cm-diameter area onto the sample.

The transducer array consisted of 192 transducers placed along a custom fabricated white ABS spherical interface containing 610 through holes with counter bores, as shown in Fig. 2(a). More holes were drilled so that the selection of the transducer positions on the ball can be flexible. The interface has an outer diameter of 160 mm and an inner diameter of 140 mm, and the diameter of the holes in the ball is 5.7 mm, which fitted well with the transducer (5.5 mm outer diameter). Each transducer (Custom designed from Blatek, Inc.) has a central frequency of 5 MHz with a reception bandwidth of greater than 80%. The active area of the transducer is 3 mm in diameter and the angular acceptance is about 15 degree. The transducers were glued onto the interface with epoxy which can be removed to allow the position change of the transducers.

There were 16 preamplifier boards separately sealed in 4 metal boxes, and each board had 12 input channels, 4 output channels, and 2 digital signal control inputs. Within each board, 12 dedicated operational amplifier modules (AD8099) individually amplify the input signals with a fixed gain of 26 dB, and then the amplified signals were multiplexed into the 4 output channels by 4 multiplexer chips (MAX 4051), which were controlled by a USB IO digital module (USB-1024LS, Measurement Computing) through the 2 digital inputs.

The 64-channel parallel data acquisition system consisted of eight 8-channel PCI cards (PCIAD850, US Ultratek) in an industrial computer. For each channel, 3000 sampling points were collected at 50 MHz sampling rate in 10 bits, and stored in a 32k on board memory before they were transferred to the host machine. Amplifiers with a programmable gain of 0 to 80 dB along with a 16 MHz low band pass filter were built into the data acquisition system. A Labview program controlled the data acquisition, and the acquired data was stored on hard disk for further image processing. Images were reconstructed with a delay-and-sum algorithm [11]. For 3D image display, the reconstructed results were normalized to 0~255 after setting the negative values to be zero. Then 3D images were rendered with Amira (from Visage Imaging, Inc.) with different thresholds as indicated in the colorbar shown in each image.

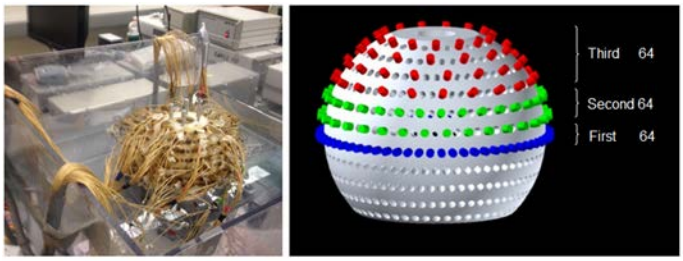

Fig. 2. The spherical transducer array. (a) Photograph of the transducer array. (b) 3D schematic of the transducer distribution on the interface.

The system allows the selection of transducer positions on the spherical interface. The total 610 holes formed 11 evenly spaced layers along the vertical direction of the ball, and the 192 transducer positions were indicated with three different colors in Fig. 2b. Three different colors were used to indicate the 3 to 1 multiplexing from the 192 transducers to the 64-channel data acquisition. This system can also be used as a real-time 2D system operating at 10 f/s using the 64 transducers arranged in the vertical center layer (blue). For *in vivo* experiments, the rat head was elevated to the center of the spherical interface through a chamber fixed at the tank bottom, whose top was about 15 mm beneath the interface center, and a transparent plastic wrap was used to cover the chamber top. For phantom experiments, a homemade silicone holder was used to hold the phantom.

#163569 - $15.00 USD Received 27 Feb 2012; revised 19 Apr 2012; accepted 15 May 2012; published 17 May 2012

3. Phantom experiments

Three different types of phantoms were used: One containing a point object for system calibration, one phantom containing three hairs tilted along different orientations for static imaging, and one phantom with ink flowing through a thin tube embedded in a phantom for real-time 3D imaging.

The point object used for calibration was a small spherical graphite particle (0.1 mm in diameter) located at the center of the spherical array and ensured an isotropic acoustic emission profile for all directions. We measured and compensated the delay of time for all the 192 channels in the radical direction, and reconstructed this point object after calibration. The hairs-containing phantom was used to demonstrate the high imaging quality of our system. Finally, we imaged an embedded tube filled with flowing ink to show the real-time imaging ability of our system. The tube had a 0.3 mm inner diameter and was horizontally placed in a phantom. No averaging of signals was performed for the phantom experiments except for the point object experiment where 10 times averaging was applied.

3.1. System characterization

We calibrated the system by recording the emission profiles from the spherical graphite particle for all the 192 channels, and then measured and compensated the time delay of each channel. We then evaluated the system resolution by reconstructing the image of the point object.

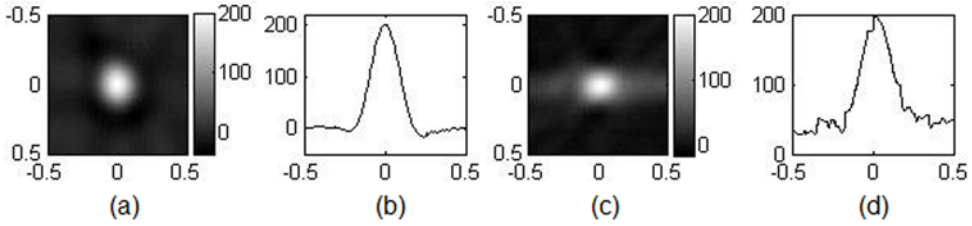

Fig. 3. (a) and (c): x-y and z-x cross section images through the center plan of the point object. (b) and (d): the profile extracted in x and z directions from (a) and (c), respectively. Units are in mm.

Figures 3a and 3c present the reconstructed x-y and z-x cross-section images of the point object located at the array center. The quality of these images is determined by both the distribution and the characteristics of the transducers. The profiles of the two reconstructed images were also extracted in x and z directions, as shown in Figs. 3b and 3d, respectively. The full width at half maximum (FWHM) of the profiles was measured to be 0.19 mm (x direction) for Fig. 3b, and 0.27 mm (z direction) for Fig. 3d, compared to the theoretical value of 0.16 mm for the 5 MHz central frequency transducer with an estimated cut off frequency of 7 MHz. It is noted that the profile in Fig. 3d is noisier than that in Fig. 3b. This along with a larger FWHM from Fig. 3d was due to the asymmetric distribution of the transducers. For targets located away from the center of the array, the radial resolution will stay nearly the same as that for a centrally located target, while the lateral resolution will be linearly reduced with increased distance away from the array center. In our system, the lateral resolution will be reduced by 0.1 mm when the target is located 5 mm off the array center.

3.2. Static phantom experiments

Figure 4a is the photograph of the phantom containing three hairs tilted along different orientations, and Figs. 4b and 4c show the reconstructed 3D images from two different views. The reconstructed volume is 10 x 10 x 10 mm with a 0.1 mm voxel size. The spatial distribution and tails for all the three hairs were clearly revealed. This result indicates that our system is capable of three-dimensionally imaging small objects of different spatial distribution and orientation in high quality.

#163569 - $15.00 USD Received 27 Feb 2012; revised 19 Apr 2012; accepted 15 May 2012; published 17 May 2012

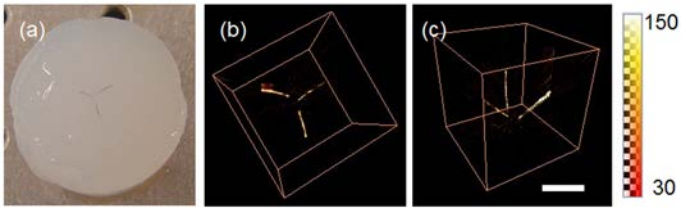

Fig. 4. (a): photograph of the phantom containing three tiled hairs; (b)-(c): reconstructed 3D images of the three hairs in two different views. Scale bar represents 5 mm.

3.3. Dynamic phantom experiments

The reconstructed 3D images of ink flowing through a thin tube are shown in Fig. 5. The image domain is 15 x 5 x 10 mm with a 0.1 mm voxel size. Figure 5a is the photograph of the phantom containing a tube filled with ink, and Figs. 5b–5j are the reconstructed 3D images at different time points. The time interval between two consecutive images was 0.3 s. These 3D images clearly tracked the flow through the tube over the course of 2.4 seconds with high spatial and temporal resolution, and the flowing speed of the ink was measured to be 6 ± 0.9 mm/s from the reconstructed results with a time interval of 0.3 s.

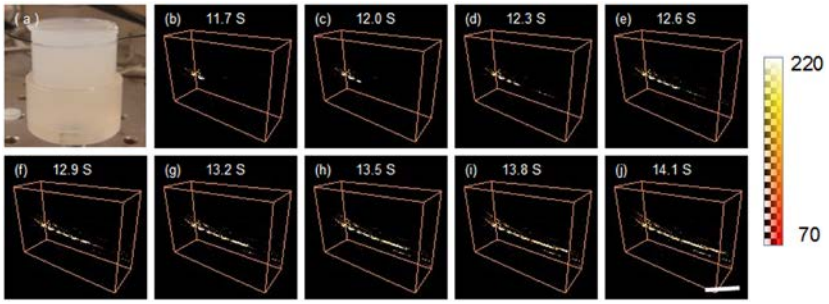

Fig. 5. Reconstructed 3D images of ink flowing through a 0.3 mm-tube embedded in a background phantom. (a): photograph of the phantom containing the tube. (b)-(j): reconstructed 3D images at different time points. The time interval is 0.3 s. Scale bar represents 5 mm.

4. Rat epilepsy experiment

Epilepsy is a serious brain disorder involving intensive hemodynamic changes, which provides high endogenous contrast for PAT imaging due to the strong absorption of blood at visible and NIR wavelengths. Compared with current existing neuron-imaging methods (such as MRI, CT, PET, and SPECT), PAT provides not only high ultrasound resolution and high optical contrast, but also unprecedented advantage of high temporal resolution over these methods, which is critical for capturing seizure dynamics.

2D PAT of seizure focus on an acute seizure rat model was demonstrated for the first time by our lab [5], but the observation of hemodynamic changes during seizure onset was hindered by the long time scanning of a single transducer. Here we test our real-time 3D system using the same animal model to show the hemodynamic changes and reveal the 3D structures in the rat brain.

Two small rats (~40g) were imaged with intact skull and skin but hairs on the head were removed. The rats were anaesthetized and mounted on the homemade plastic chamber/holder. Focal seizure was induced by microinjection of 10 μl of 1.9 mM bicuculline methiodide (BMI) into the neocortex of one rat, while saline solution was injected into the brain of another rat as control. In each experiment, the rat was elevated to the transducer array center and kept alive under the water tank through the whole experiment. The incident energy of the 730 nm light was maintained at 8mJ/cm^2 below the safety standard. Seizure process was recorded for 50 minutes, and the measurement from the control rat was recorded for 3 s. All

#163569 - $15.00 USD Received 27 Feb 2012; revised 19 Apr 2012; accepted 15 May 2012; published 17 May 2012

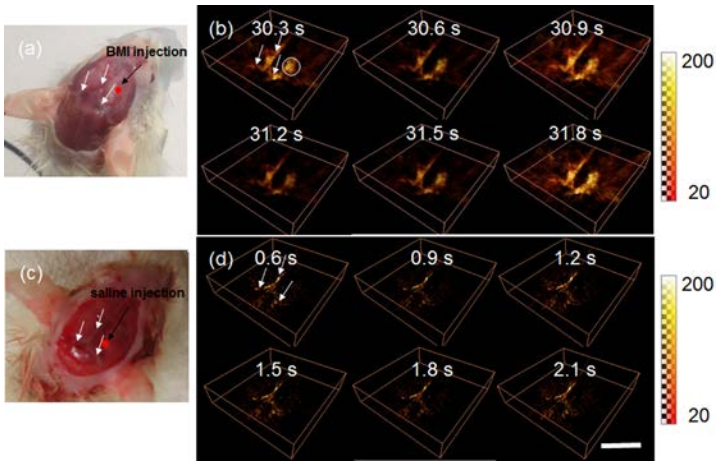

Fig. 6. (a) and (c): photograph of the rat with BMI injection and the control rat after scalp removed. (b) and (d): 3D PAT images at 6 time points for (a) and (c) respectively. The three main blood vessels are indicated by the white arrows, and the seizure focus is indicated by the circle in (b). The time interval between two successive images is 0.3 s. Scale bar represents 10 mm.

animal procedures were performed in accordance with the approved University of Florida IACUC protocols.

Figure 6b presents the 3D images for the rat with BMI injection during the seizure onset at 6 time points, compared with that for the control rat in Fig. 6b. The corresponding photographs of the two rats with scalp removed right after the experiments are shown in Figs. 6a and 6c, respectively. The reconstructed domain for the images shown in both Figs. 6b and 6d is 20 x 20 x 4.5 mm, with a 0.1 mm pixel size. The three main blood vessels on the rat brain are clearly revealed for both cases, as indicated by the white arrows, and for the rat with BMI injection a seizure focus can be clearly seen right at the BMI injection position (the white circle in Fig. 6b), where strong absorption is observed during seizure onset. The rapid changes of the absorption both in the main blood vessel and in the seizure focus were observed from Fig. 6b, while no such changes were noted for the control rat (Fig. 6c). The seizure focus had a diameter of ~3 mm, which is consistent with the results published before [5]. This experiment demonstrates that our system can be used to investigate the hemodynamic changes in small animal brain both spatially and temporally during seizure onset, although the complex microvasculature cannot be resolved due to the limited number of transducers and the simple backprojection reconstruction method used here. The microvasculature can be revealed if sophisticated reconstruction methods such as the finite element based algorithms coupled with the total variation minimization scheme are used [12,13].

5 Conclusions

We have presented a real-time photoacoustic system for three-dimensionally imaging focal cortical seizures in a rat. The system is based on a spherical array containing 192 discrete transducers. With the 64-channel data acquisition system coupled with 3:1 multiplexing, it can achieve a frame rate of 3.3 f/s with a spatial resolution of 0.2 mm. The 3D imaging performance of the system was demonstrated by both static and dynamic phantom experiments. We have also tested our system using an acute epilepsy rat model and obtained 3D images showing the hemodynamic changes during seizure onset.

Acknowledgments

This research was supported in part by a grant from the U.S. Department of Defense Congressionally Directed Medical Program, the B.J. and Eve Wilder endowment fund, and the Children's Miracle Network.

#163569 - $15.00 USD Received 27 Feb 2012; revised 19 Apr 2012; accepted 15 May 2012; published 17 May 2012